Heliyon 9 (2023) e15696

Contents lists available at ScienceDirect

Heliyon

journal homepage: www.cell.com/heliyon

Research article

Computational analysis of Darcy-Forchheimer relation, reduced gravity, and external applied magnetic field influence on radiative fluid flow and heat transfer past a sphere: Finite difference method

Amir Abbas [a], Muhammad Ashraf [b], Hafeez Ahmad [c], Kaouther Ghachem [d], Zia Ullah [e], Abid Hussanan [f], Taher Labidi [g], Lioua Kolsi [h,i,*]

[a] Department of Mathematics, Faculty of Science, University of Gujrat, Sub-Campus, Mandi Bahauddin, 50400, Pakistan
[b] Department of Mathematics, Faculty of Science, University of Sargodha, Sargodha, 40100, Pakistan
[c] Department of Statistics, School of Quantitative Sciences, University of Utara, Malaysia
[d] Department of Industrial Engineering and Systems, College of Engineering, Princess Nourah bint Abdulrahman University, P.O. Box 84428, Riyadh, 11671, Saudi Arabia
[e] Department of Mathematics and Statistics, Faculty of Science, Sargodha-Campus, The University of Lahore, Sargodha, 40100, Pakistan
[f] Department of Mathematics, Division of Science and Technology, University of Education, Lahore, 54000, Pakistan
[g] Department of Software Engineering, College of Computer Engineering and Sciences, Prince Sattam bin Abdulaziz University, P.O. Box 151,Al-Kharj, 11942, Saudi Arabia
[h] Department of Mechanical Engineering, College of Engineering, University of Ha'il, Ha'il City, 81451, Saudi Arabia
[i] Laboratory of Metrology and Energy Systems, Department of Energy Engineering, University of Monastir, Monastir, 5000, Tunisia

ARTICLE INFO

Keywords:
Darcy-Forchheimer relation
Reduced-gravity
Magnetohydrodynamics
Finite difference method
Solar-radiation
Porous-medium
Sphere

ABSTRACT

The study of radiation, Darcy-Forchheimer relation, and reduced gravity, effects on magneto-hydrodynamic flow across a solid sphere immersed in porous material, is the focus of the current work. Coupled and nonlinear partial differential governing equations, are established to model the studied configuration. By using appropriate scaling variables, the resultant set of governing equations is converted to its dimensionless form. Based on these established equations, a numerical algorithm is written based on the finite element approach to solve the considered problem. A verification of the validity of the proposed model is done by comparing with already published results. Furthermore, to check the precision of solutions, a grid independence test has been accomplished. The unknown variables, such as fluid velocity and temperature, and their gradients are evaluated. This investigation's main objective is to demonstrate how the Darcy-Forchheimer law and reduced gravity due to density difference affect the natural convective heat transfer across a solid sphere immersed in a porous medium. Results show that the flow intensity decreases with the magnetic field parameter, local inertial coefficient, Prandtl number, and porosity parameter and becomes more important by increasing the reduced gravity and radiation parameters. In addition, the temperature increases with the inertial coefficient, porosity parameter, Prandtl number, radiation parameter, and magnetic field parameter and get declined with the reduced gravity parameter.

* Corresponding author. Department of Mechanical Engineering, College of Engineering, University of Ha'il, Ha'il City, 81451, Saudi Arabia.
E-mail addresses: cfdamirabbas4693@gmail.com (A. Abbas), muhammad.ashraf@uos.edu.pk (M. Ashraf), ranahafeez608@gmail.com (H. Ahmad), kgmaatki@pnu.edu.sa (K. Ghachem), ziakhan.uos.72@gmail.com (Z. Ullah), abid.hussanan@ue.edu.pk (A. Hussanan), t.labidi@psau.edu.sa (T. Labidi), l.kolsi@uoh.edu.sa (L. Kolsi).

https://doi.org/10.1016/j.heliyon.2023.e15696
Received 21 January 2023; Received in revised form 13 April 2023; Accepted 19 April 2023
Available online 25 April 2023

1. Introduction

The fluid flow and heat transfer processes in porous media become the focus of the research community and engineers due to their manifestation in diverse engineering applications. Such as in packed beds, fossil fuel beds, nuclear, resin transfer models, geothermal energy, and waste disposal. According to Darcy's law, average velocity and pressure gradients are directly dependent on each other. In literature, these problems grabbed lot of attention. Darcy's law is valid only if porosity and velocity levels are low. Darcy and Elizabeth's relationship is meaningless because of the uneven porosity and higher velocities as demonstrated by diverse industrial and technological systems. Thus, to get better accuracy, it is highly recommended that the model of the flow in porous media be non-Darcian. Forchheimer's law combines both inertial effects and high-speed flow. Because it combines Darcy's component's non-degeneracy and the monotonicity of nonlinear term, Forchheimer's law is exceptional. Forchheimer's [1] computation of Darcy's velocity includes the square velocity factor in order to analyze the characteristics of inertia and boundary. ''Forchheimer'' term, is always used to describe problems with high Reynolds number values [2]. Upreti et al. [3]applied the 3D Darcy-Forchheimer law on CNT-nanofluid flow past stretchable surface while considering the Ohmic heating and heat generation/absorption effects. Generalized transfer laws coupled with Williamsons equations were utilized by Ramzan et al. [4] to study nanofluid MHD flow past a sheet immersed in a porous medium. Hayat et al. [5] used the Darcy-Forchheimer law to investigate the double diffusive convection during a non-Newtonian fluid. Based on the Darcy-Forchheimer theory, Upreti et al. [6] studied the radiative Sisko nanofluid flow along a stretching sheet immersed in a porous medium. Sadiq et al. [7] did research on chemically reacting, radiative convective process past a stretching sheet with the consideration of the Darcy-Forchheimer law. Khan et al. [8] performed a study on Lorentz force influence Darcy-Forchheimer flow of Carreau-Yasuda nanofluid. Nagaraja et al. [9] performed an investigation on the chemically reacting, radiative Jeffery nanofluid flow due to stretching sheet with convective conditions. Researchers in Refs. [10–12] adopted the Darcy–Forchheimer law to study the flows of different fluids through various geometries.

Industry must use light mechanical equipment in order to attain the high levels of accuracy, speed, and acceleration made available by cutting-edge technology. A sphere is an illustration of an inventive, lightweight engineering device that lowers the quantity of heavy moving parts in a machine and examines the momentum and thermal boundary layer. Metal and alloy devices with sphere shapes are employed as components in mechanical systems in various industrial processes. Riley [13] discussed natural convection past a sphere. In order to study the oscillatory heat transfer mechanisms past a sphere, Ashraf et al. [14] considered several kinds of fluids. In the work on Ashraf and Fatima [15] a time dependent heat transfer process with dissipation impact was carried out. In the paper of Ashraf et al. [16] the natural convection of a nanofluid in the plume region around a sphere was discussed. Some other studies [17–21] considered the convective heat transfer around spheres for various kinds of fluids. Ahmad et al. [22] employed the FEM in order to solve the equations governing the convection over a curved plate with the consideration of the chemical reaction effect.

Thermal radiation is the kind of heat transfer caused by the propagation of electromagnetic waves. In this heat transfer mode, no medium is required like in conduction and convection. Cortell [23] investigated the combined radiation and convection over a horizontal moving surface. There have been some studies [24–27]on the Sakiadis and Balsius flow under magnetic and thermal radiation effects for various kinds of fluid.

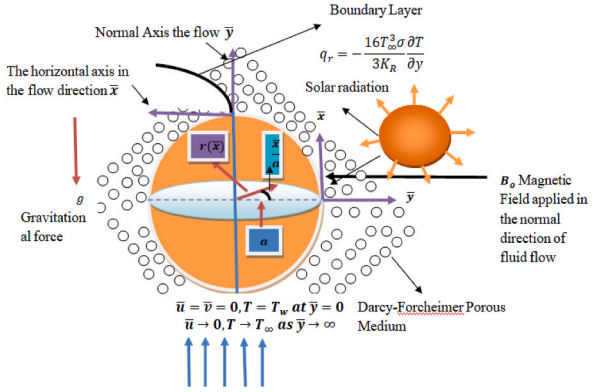

Fig. 1. Studied configuration

$$\frac{\partial(\bar{r}u)}{\partial\bar{x}} + \frac{\partial(\bar{r}v)}{\partial\bar{y}} = 0 \tag{1}$$

$$\bar{u}\frac{\partial\bar{u}}{\partial\bar{x}} + \bar{v}\frac{\partial\bar{u}}{\partial\bar{y}} = \nu\frac{\partial^2\bar{u}}{\partial\bar{y}^2} + g\frac{\rho - \rho_\infty}{\rho_\infty}\sin\frac{\bar{x}}{a} - \frac{\sigma B_0^2}{\rho}u - \frac{\nu}{K_o}\bar{u} - F_1u^2 \tag{2}$$

$$\bar{u}\frac{\partial T}{\partial\bar{x}} + \bar{v}\frac{\partial T}{\partial\bar{y}} = \alpha_m\frac{\partial^2 T}{\partial\bar{y}^2} - -\frac{1}{\rho C_p}\frac{\partial q_r}{\partial y} \tag{3}$$

Magnetic field effects on heat transfer have several applications in engineering, physics, and chemistry, such as the MHD pumps, process of boundary layer and bearings in electrically conducting fluid, power generation and geophysics. Tamoor et al. [28] studied the MHD Casson flow on the surface of a stretchable cylinder. The combined influence of magnetic force and chemical reacting on the fluid flow through a surface stretching in exponential manner have been performed by Pattnaik et al. [29]. Mabood et al. [30], performed a computational evaluation of the radiative magnetohydrodynamic flow over exponentially stretched plate employing the homotopy analysis technique. Salahuddin et al. [31] studied the MHD Williamson fluid flow past a stretchable geometry having variable thickness. Kumar et al. [32] investigated the effects of generation/absorption of heat, and Lorentz force on convective flow. In Refs. [33,34], investigations on magnetohydrodynamic flow past various shapes can be found. Kuiken and Merkin [35]conducted a study on transfer of heat due to heated bars with reduced gravity. Due to its significance in the fields of nature and science, natural convection piqued the concentration of the research community. It is particularly observed in plumes that rise from hot air generated by fire, ocean currents, etc. It is quite interesting to study the physics of lower gravity. Sparrow and Gregg [36] studied the convective flow past flat plate for small values of Prandtl number. Studies on the phenomena of free convection over different geometries are discussed in Refs. [37–42].

Based on the above presented literature review it is noticed that radiation, Darcy-Forchheimer relation, magnetohydrodynamics, and reduced gravity, effects on along a sphere contained in a porous material has not been considered before the current attempt. The entire solution process of the constructed model is provided in the next part, and the results for the relevant properties are shown in terms of graphs and tables along with a thorough explanation and justification.

2. Flow configuration and governing equations

The considered configuration (Fig. 1) consists of an incompressible, viscous, steady, and two-dimensional external flow of fluid past a sphere immersed in a porous medium. Here, x-axis designates flow direction and y-axis is normal to it. Velocity components are (u, v) are in x *and* y direction, respectively. The Darcy-Forcheimer relation along with solar radiation effects are considered. A Magnetic field perpendicular to fluid flow is applied with a strength B_o. T_w is the surface temperature and T_∞ is the ambient temperature with $T_w > T_\infty$. The fluid is considered to be optically dense gray. By following [1,2,13,23,&35]], the flow model is presented as follow:

Here, $\bar{u}$ and $\bar{v}$ denote velocity components in $\bar{x}$ and $\bar{y}$ axises, and $\bar{r} = a \sin\frac{\bar{x}}{a}$ is radial distance that stems from symmetric axis to surface. The designations ρ is density of fluid, a is sphere radius, ν is kinematic viscosity, K_o is porous medium permeability, B_o is strength of magnetic field, α_m is thermal diffusivity, and σ is electrical conductivity. Here, $F_1 = \frac{C_b}{\sqrt{K_1}}$ is coefficient of inertia with C_b is the drag coefficient.

By following [23], the radiative heat flux q_r is:

$$q_r = -\frac{4\sigma_s}{3k^*}\frac{\partial T^4}{\partial y}. \tag{4}$$

Here, σ_s k^* are constant of Stefan-Boltzmann and mean absorption coefficient. With:

$$T^4 \approx 4T_\infty^3 T - 3T_\infty^4.$$

By following [23], equation (4) becomes:

$$q_r = -\frac{16T_\infty^3\sigma_s}{3K_R}\frac{\partial T}{\partial y} \tag{5}$$

Now equation (3) obtains the form that is given in [23].

$$u\frac{\partial T}{\partial x} + v\frac{\partial T}{\partial y} = \frac{k_\infty}{\rho C_p}\frac{\partial^2 T}{\partial y^2} + \frac{16T_\infty^3\sigma_s}{\rho C_P 3K_R}\frac{\partial^2 T}{\partial y^2}, \tag{6}$$

Equation (6) implies the following that is given in [23].

$$u\frac{\partial T}{\partial x} + v\frac{\partial T}{\partial y} = \frac{k}{\rho C_p}\frac{\partial}{\partial y}\left[\frac{\partial T}{\partial y} + \frac{4.4\ T_\infty^3\sigma_s}{\rho C_P 3kK_R}\frac{\partial T}{\partial y}\right], \tag{7}$$

By following [35], temperature T_m and density ρ_m relation is given in Eq. (8)

$$\frac{\rho - \rho_m}{\rho_m} = -\gamma(T - T_m)^2 \tag{8}$$

By following [35], Eq. (6) implies for steady flow:

$$T \to T_m \pm \Delta T y \to \pm \infty \tag{9}$$

By following [35], boundary conditions are.

$$\overline{u} = 0, \overline{v} = 0, T = T_m \text{ at } y = 0, \overline{u} \to 0, T \to T_\infty \text{ as } y \to \infty \tag{10}$$

By following [35], T_∞ and ρ_∞ relation is given in Eq. (8), so reduced gravity is expressed as:

$$g' = g\frac{(\rho_m - \rho_\infty)}{\rho_\infty} \tag{11}$$

By following [35], fluid particles acceleration which has density ρ_m. From Eq. (8)

$$g' = g\gamma\frac{\rho_m}{\rho_\infty}(T_\infty - T_m)^2 \tag{12}$$

3. Resolution procedure

In the following sub-sections, the procedure of establishing the dimensionless equations, then transformation for smooth algorithm and at the end the employed solution scheme is discussed in detail.

3.1. Dimensionless formulation

To determine the solutions of Eqs. (1)–(3) along with Eq. (10), a dimensional analysis process is adopted to establish the dimensionless set of equations. The dimensionless variables are given in Eq. (13) used by Ref. [19]:

$$x = \frac{\overline{x}}{a}, y = \frac{\overline{y}Gr^{\frac{1}{4}}}{a}, \theta = \frac{T - T_\infty}{T_m - T_\infty}, u = \frac{a\overline{u}Gr^{\frac{1}{4}}}{\nu}, v = \frac{a\overline{v}Gr^{\frac{1}{4}}}{\nu}, \tag{13}$$

Following [1,2,13,19,23,35] Eqs. (1)–(3) with (10) takes the following form when Eq. (13) is used,

$$\frac{\partial(\sin xu)}{\partial x} + \frac{\partial(\sin xv)}{\partial y} = 0, \tag{14}$$

$$u\frac{\partial u}{\partial x} + v\frac{\partial u}{\partial y} = \frac{\partial^2 u}{\partial y^2} + R_g(2\theta - \theta^2)sinx - Du - Hu - F\,u^2, \tag{15}$$

$$u\frac{\partial \theta}{\partial x} + v\frac{\partial \theta}{\partial y} = \frac{1}{Pr}\left(1 + \frac{4}{3}N_r\right)\frac{\partial^2 \theta}{\partial y^2}, \tag{16}$$

$$u = 0, v = 0, \theta = 1, \text{at } y = 0, u \to 0, \theta \to 0, \text{as } y \to \infty. \tag{17}$$

Here, $F = \frac{C_b Gr^{\frac{1}{4}}}{\sqrt{K_1}}$ is local inertial coefficient, $H = \frac{\sigma B_o^2 a^2 Gr^{\frac{1}{4}}}{\rho\nu}$ is magnetic field parameter, $R_g = \frac{g'}{g\,\beta\Delta T}$ is reduced gravity parameter with g' is reduced gravity acceleration, $D = \frac{a^2 Gr^{\frac{1}{4}}}{K_o}$ is porosity parameter, $\Pr = \frac{\nu}{\alpha}$ is Prandtl number, and $, N_r = kK_R/4\sigma^* T_\infty^3$ is radiation parameter.

3.2. Formulation of primitive variables

For the smoothness of numerical algorithm of the modeled problem in FORTRAN, Eqs. 14–16 along with modeled Eq. (17), following [19] the transformation variables given in Eq. (18) are employed.

$$u(x,y) = x^{1/2}U(X,Y), v(x,y) = x^{-\frac{1}{4}}V(X,Y), \mathrm{Y} = x^{-\frac{1}{4}}y, X = x, \theta(x,y) = \theta(\mathrm{X},\mathrm{Y}) \tag{18}$$

Following [1,2,13,19,23,35] Eqs. 14–16 along with modeled Eq. (17), takes the following after using Eq. (18)

$$\mathrm{XU}\,\cos\mathrm{X} + \left(\mathrm{X}\frac{\partial \mathrm{U}}{\partial \mathrm{X}} - \frac{\mathrm{Y}}{2}\frac{\partial \mathrm{U}}{\partial \mathrm{Y}} + \frac{\partial \mathrm{V}}{\partial \mathrm{Y}}\right)\sin\mathrm{X} = 0, \tag{19}$$

$$XU\frac{\partial U}{\partial X} + \frac{1}{2}U^2 + \left(V - \frac{YU}{2}\right)\frac{\partial U}{\partial Y} = \frac{\partial^2 U}{\partial Y^2} + R_g(2\theta - \theta^2)\mathrm{sinX} - \mathrm{HU} - \mathrm{DU} - \mathrm{FU}^2, \tag{20}$$

$$XU\frac{\partial\theta}{\partial X}+\left(V-\frac{YU}{2}\right)\frac{\partial\theta}{\partial Y}=\frac{1}{Pr}\left(1+\frac{4}{3}N_r\right)\frac{\partial^2\theta}{\partial Y^2}, \tag{21}$$

The boundary conditions are:

$$U=0, V=0, \theta=1, \text{at } Y=0, U\to 0, \theta\to 0, \text{as } Y\to\infty. \tag{22}$$

3.3. Solution scheme

Equations 19–21 with (22) are discretized utilizing the FEM. In X-axis direction first order backward difference is applied, and in Y-axis first and second order central difference is applied. Here, $(U_{i,j}, V_{i,j}, \theta_{i,j})$ are unknown discretized variables. By using the above-mentioned method to Equations 19–21 with (22) by adopting the solution process given in [19]

Discretized continuity equation

$$V_{(i+1,j)}=V_{(i-1,j)}-2\frac{\Delta Y}{\Delta X}X_i\left(U_{(i,j)}-U_{(i,j-1)}\right)+\frac{Y_j}{2}\left(U_{(i+1,j)}-U_{(i-1,j)}\right)$$

$$-2\Delta Y X_i\frac{cos\ X_i}{\sin X_i}U_{(i,j)} \tag{23}$$

Discretized Momentum Equation

$$\left(1+\frac{\Delta Y}{2}\left(V_{(i,j)}-\frac{Y_j}{2}U_{(i,j)}\right)\right)U_{(i-1,j)}+\Bigg(-2-\frac{\Delta Y^2}{\Delta X}X_iU_{(i,j)}-H-D-FU_{(i,j)}\Bigg)U_{(i,j)}+\left(1-\frac{\Delta Y}{2}\left(V_{(i,j)}-\frac{Y_j}{2}U_{(i,j)}\right)\right)U_{(i+1,j)}=-\Delta Y^2\ sin\ X_iR_g\left(2\theta_{(i,j)}-\theta^2_{(i,j)}\right), \tag{24}$$

Discretized Energy Equation

$$\left(\frac{1}{Pr}\left(1+\frac{4}{3}N_r\right)+\frac{\Delta Y}{2}\left(V_{(i,j)}-\frac{Y_j}{2}U_{(i,j)}\right)\right)\theta_{(i-1,j)}+\Bigg(-\frac{2}{Pr}\left(1+\frac{4}{3}N_r\right)+\Delta Y^2U_{(i,j)}\left(1-\frac{X_i}{\Delta X}\right)\Bigg)\theta_{(i,j)}+\left(\frac{1}{Pr}\left(1+\frac{4}{3}N_r\right)-\frac{\Delta Y}{2}\left(V_{(i,j)}-\frac{Y_j}{2}U_{(i,j)}\right)\right)\theta_{(i+1,j)}=-\frac{\Delta Y^2}{\Delta X}X_iU_{(i,j)}\theta_{(i,j-1)}, \tag{25}$$

By following [19] the discretized boundary conditions become:

$$U_{i,j}=0, V_{i,j}=0, \theta_{i,j}=1, \text{at } Y_j=0,$$

$$U_{i,j}\to 0, \theta_{i,j}\to 0, \text{as } Y_j\to\infty. \tag{26}$$

For accuracy of solution, the convergence criterion for U, V and and θ variables, is given below:

$$\max\left|U_{ij}\right|+\max\left|V_{ij}\right|+\max\left|\theta_{ij}\right|\le\varepsilon$$

Where, $\varepsilon=10^{-5}$. Here, in this simulation step size has taken as $\Delta X=0.05$ and $\Delta Y=0.02$. A computation is started from $X=0$ to infinity. The results are elaborated in the next sections.

Table 1
Mesh analysis or mesh independence test for $H=1.0, N_r=1.0, R_g=10.0, \Pr=7.0$, $D=0.1$, $F=0.1$ at $X=\pi/4$.

Grid points	$\left(\frac{\partial U}{\partial Y}\right)_{Y=0}$	$-\left(\frac{\partial\theta}{\partial Y}\right)_{Y=0}$
25	3.22837	0.97809
50	3.33500	0.92792
100	3.34338	0.92006
125	3.34357	0.91955
200	3.34358	0.91920
250	3.34359	0.91916
300	3.34361	0.91915
350	3.34361	0.91915
400	3.34361	0.91915

4. Model verification and grid sensitivity test

In Table 1, the test of grid independence test is presented by considering various grid points for Y = 10.0. The solution is more accurate for finer grids. Additionally, the findings deviation for heat transfer rate and skin friction at position $X = \pi/4$ has been calculated from grid points 200 to 400. From the computed results for skin friction, it is noted that the results deviation percentage is 0.0008% and for heat transfer rate is 0.005%. The usage of 200 grid points is adequate for the convergence and correctness of the results calculated using the finite difference method, it may be inferred from the deviation of the computed results. Utilizing 200 grid points, the whole set of solutions for the current model is established. For this grid independent test, the magnetic field parameter is $H = 1.0$, radiation parameter $Rd = 1.0$, reduced gravity parameter $R_g = 10.0$, local inertial coefficient $F = 0.1$, porosity parameter $D = 0.1$, and Prandtl number $Pr = 7.0$ at $X = \pi/4$.

5. Results and discussion

Numerical outcomes of hypothesized phenomena are thoroughly elaborated in the current section. The velocity, temperature, $\partial U/\partial Y$ and $\partial\theta/\partial Y$ for various parametric values of reduced gravity number R_g, radiation parameter N_r, and magnetic field parameter H, porosity parameter D, local inertial coefficient F, and Prandtl number Pr, are calculated and shown as tables and graphs. Figs. 2–3 illustrate the impact of the local inertial coefficient on the velocity field and temperature distribution at distinct locations outside the sphere surface. Graphical results indicate that the intensification of F causes the reduction of the velocity and the augmentation of the temperature for all the considered positions. The impact of the reduced gravity number R_g on the velocity profile U for Pr = 7.0 is shown in Fig. 4 at various points on the sphere. The Graph shows that as R_g increases, the velocity values become more important. Fig. 5 depicts the temperatures profiles for various R_g values. The temperature curves at various circumferential points, show that as R_g is amplified, the fluid temperature quickly decreases. The highest temperature value occurs at $X = \pi$. The effects the porosity parameter D on the velocity field are highlighted in Fig. 6. It is noticed that the velocity rises with D is at all the points. The effect of D on the temperature field is depicted in Fig. 7. As D increases, the fluid temperature becomes higher. The numerical findings of U versus different values of Pr are depicted in Fig. 8. At all the considered positions the velocity drops as Pr value is raised, and the maximum velocity is reached at $X = \pi/2$. Fig. 9 illustrates how Randtl number affects the fluid's temperature. It is noticed that the temperature values are inversely proportional to Prandtl number. This is due to the lower values of the conductivity when Pr increases, which causes a reduction of the exchanged heat and consequently lower temperatures. The fluid velocity and temperature profiles, for a range of values of radiation number N_r at different locations, are shown in Figs. 10 and 11. Both the velocity and temperature increase when N_r values increase. Figs. 12 and 13 illustrate the effect of the magnetic field magnitude on the velocity and temperature fields, respectively. It is noticed that the velocity is diminishing, and the temperature is augmenting with the amplification in H. Due to the generation of the Lorentz force that opposes the convection, a retardation in the flow intensity occurs and causes the reduction the velocity magnitude.

Table 2 presents a comparison of the current solution of the skin friction with previously published solutions [36] for fixed reduced gravity terms. The tabular solutions demonstrate that there is excellent agreement between the two, which supports the validation of the simulation of the existing model. Table 3 is showing the solutions of $\partial U/\partial Y$ and $\partial\theta/\partial Y$ versus the porosity parameter D. An increasing of the value of D causes to weak the of skin friction and heat transfer rate at all the circumferential points of the sphere. Table 4 is showing $\partial U/\partial Y$ and $\partial\theta/\partial Y$ at distinct locations. It is noticed that both quantities decrease gradually with the augmentation of magnetic field parameter H. This is due to the produced Lorentz force that reduces the thermal buoyancy.

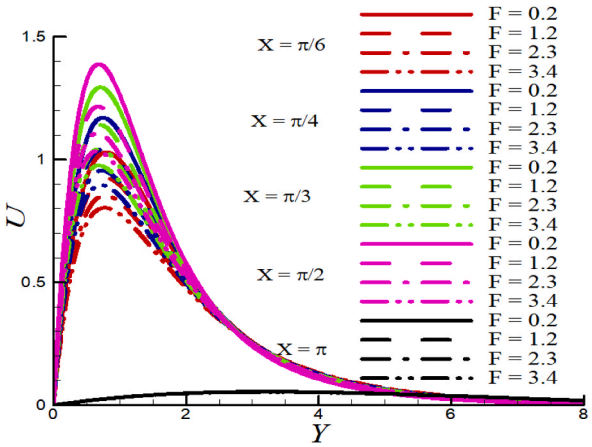

Fig. 2. Impact of F on U when Pr = 7.0, $N_r = 1.0$, $H = 1.0$, and $D = 0.1$.

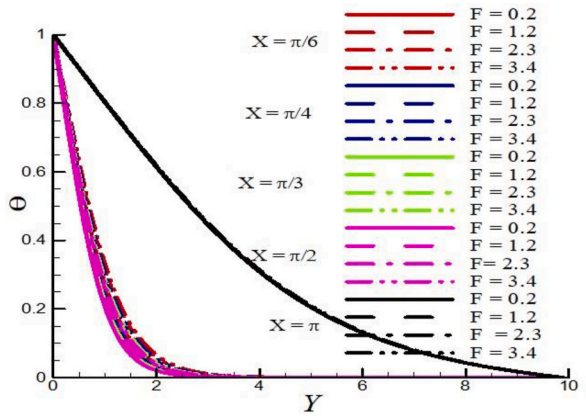

Fig. 3. Impact f F on θ when $R_g = 10.0,\ \mathrm{Pr} = 7.0,\ N_r = 1.0,\ H = 1.0$, and $D = 0.1$.

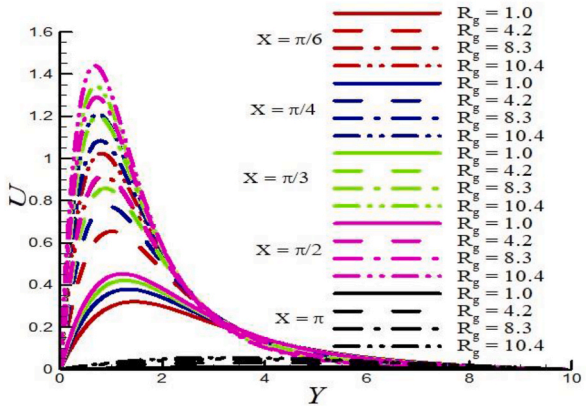

Fig. 4. Impact of R_g on U when $F = 0.1,\ \mathrm{Pr} = 7.0,\ N_r = 1.0,\ H = 1.0$, and $D = 0.1$.

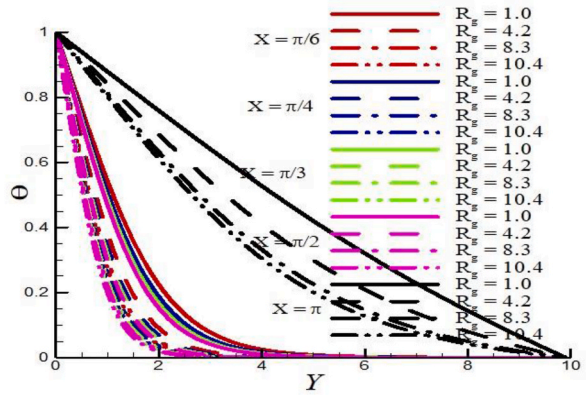

Fig. 5. Impact of R_g on θ when $F = 0.1,\ \mathrm{Pr} = 7.0,\ N_r = 1.0,\ H = 1.0$, and $D = 0.1$.

6. Concluding remarks

The impact of radiation, Darcy-Forchheimer relation, reduced gravity, and magnetohydrodynamics on natural convection past a stationary sphere submerged in a fluid is discussed in the current paper. The main findings are summarized as follow:

- The solutions reflect that the velocity is proportional to the reduced gravity parameter, and radiation parameter but inversely proportional to the magnetic field parameter, local inertial coefficient, Prandtl number, and porosity parameter.

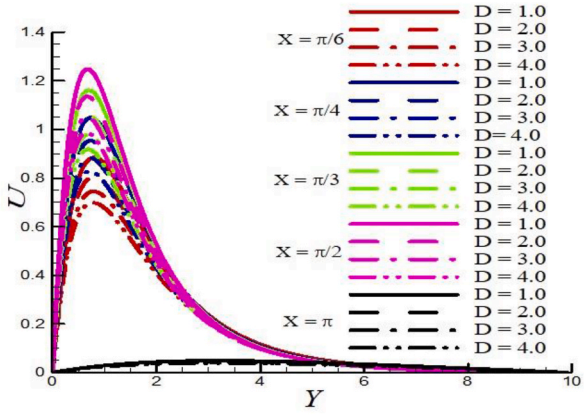

Fig. 6. Impact of D on U when $Fr = 0.1,\ \mathrm{Pr} = 7.0$, $N_r = 1.0$, $H = 1.0$, and $R_g = 10.0$.

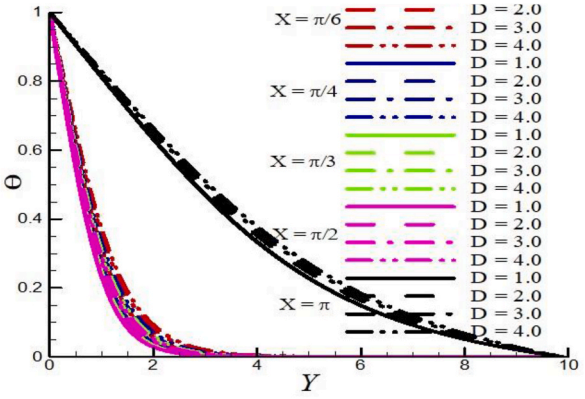

Fig. 7. Impact of D on θ when $F = 0.1,\ \mathrm{Pr} = 7.0$, $N_r = 1.0,\ = 1.0$, and $R_g = 10.0$.

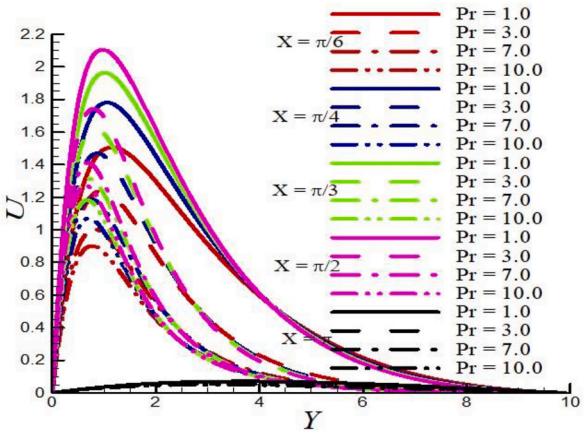

Fig. 8. Impact of Pr on U when $F = 0.1, D = 0.1$, $N_r = 1.0$, $H = 1.0$, and $R_g = 10.0$.

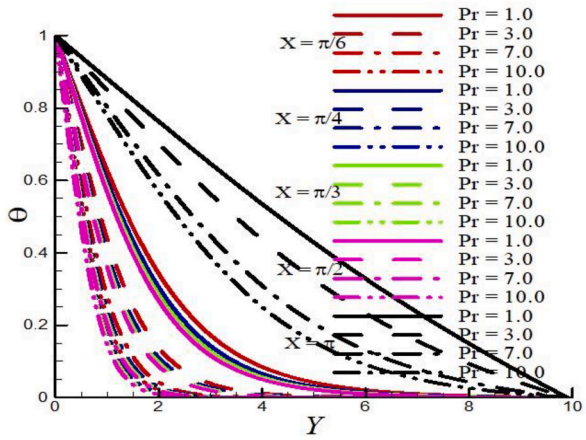

Fig. 9. Impact of Pr on θ when $F = 0.1, D = 0.1$, $N_r = 1.0$, $H = 1.0$, and $R_g = 10.0$.

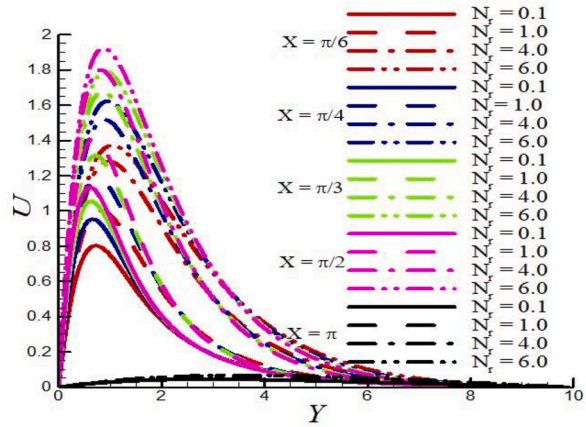

Fig. 10. Impact of N_r on U when $F = 0.1, D = 0.1$, $Pr = 7.0$, $H = 1.0$, and $R_g = 10.0$.

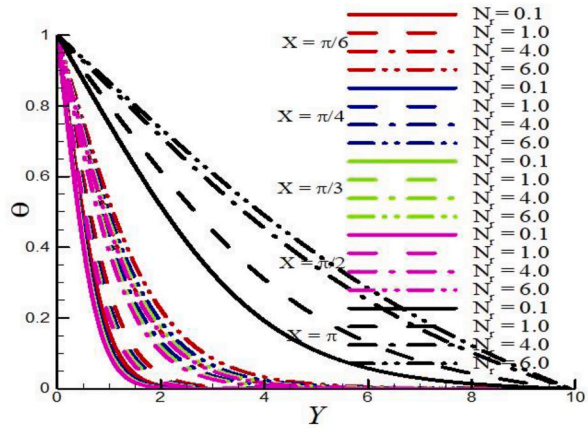

Fig. 11. Impact of N_r on U when $F = 0.1, D = 0.1$, $Pr = 7.0$, $H = 1.0$, and $R_g = 10.0$.

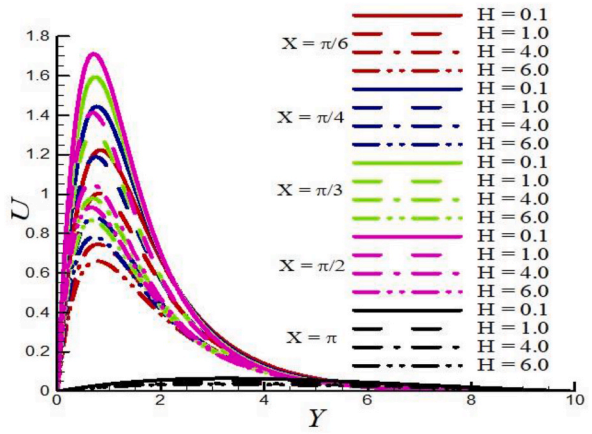

Fig. 12. Impact of H on U when $F = 0.1, D = 0.1$, $Pr = 7.0$, $N_r = 1.0$, and $R_g = 10.0$.

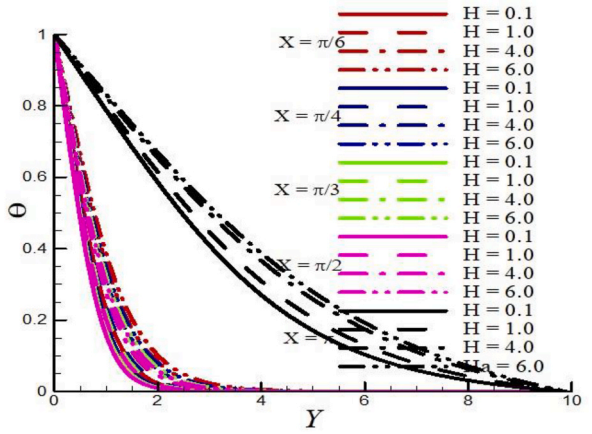

Fig. 13. Impact of H on θ when $F = 0.1, D = 0.1$, $Pr = 7.0$, $N_r = 1.0$, and $R_g = 10.0$.

Table 2

Validation of present study with previously published results for $\left(\frac{\partial U}{\partial Y}\right)_{Y=0}$ in absence of reduced gravity and for $H = 0.0, N_r = 0.0, \mathrm{D} = 0.0, \mathrm{F} = 0.0$ at $\pi/2$.

Pr	Sparrow & Gregg [36]	Present results
0.03	0.93841	0.93740
0.02	0.95896	0.95870
0.008	0.99550	0.99400

- The temperature increases with the inertial coefficient, parameter porosity, Prandtl number, radiation parameter, and magnetic field parameter and declines with the reduced gravity parameter.
- There is a reduction in the skin friction and heat transfer when the porosity parameter and magnetic field parameters are augmented.
- The solutions of the current model are in good concordance with previously published findings.
- A grid independence test is performed to demonstrate the reliability of the solutions.

Author contribution statement

Amir Abbas; Muhammad Ashraf: Conceived and designed the experiments; Performed the experiments; Analyzed and interpreted the data; Wrote the paper.

Hafeez Ahmad: Performed the experiments; Analyzed and interpreted the data; Wrote the paper.

Kaouther Ghachem: Analyzed and interpreted the data; Wrote the paper.

Table 3

Impact of the permeability parameter D on a) $\left(\frac{\partial U}{\partial Y}\right)_{Y=0}$ b) $-\left(\frac{\partial \theta}{\partial Y}\right)_{Y=0}$ when $F = 0.1,\ \mathrm{Pr} = 7.0$, $N_r = 1.0$, and $H = 1.0$, $R_g = 10.0$.

X	$\left(\frac{\partial U}{\partial Y}\right)_{Y=0}$			
	$D = 1.0$	$D = 2.0$	$D = 3.0$	$D = 4.0$
$\pi/6$	2.72824	2.57326	2.45555	2.36128
$\pi/4$	3.52303	3.32373	3.17211	3.05057
$\pi/3$	4.11516	3.88301	3.70622	3.56441
$\pi/2$	4.58198	4.32404	4.12745	3.96968
π	0.03630	0.03425	0.03269	0.03144
X		$-\left(\frac{\partial \theta}{\partial Y}\right)_{Y=0}$		
	$D = 1.0$	$D = 2.0$	$D = 3.0$	$D = 4.0$
$\pi/6$	0.78858	0.75302	0.72528	0.70260
$\pi/4$	0.85840	0.81985	0.78974	0.76510
$\pi/3$	0.90378	0.86331	0.83167	0.80576
$\pi/2$	0.93655	0.89470	0.86196	0.83515
π	0.18777	0.18102	0.17585	0.17170

Table 4

Impact of the magnetic field parameter H on a) $\left(\frac{\partial U}{\partial Y}\right)_{Y=0}$ b) $-\left(\frac{\partial \theta}{\partial Y}\right)_{Y=0}$ when $F = 0.1, D = 0.1$, $Pr = 7.0$, $N_r = 1.0$, and $R_g = 10.0$.

X	$\left(\frac{\partial U}{\partial Y}\right)_{Y=0}$			
	$H = 0.1$	$H = 1.0$	$H = 4.0$	$H = 6.0$
$\pi/6$	3.34350	2.95154	2.45555	2.28306
$\pi/4$	4.30772	3.80934	3.17211	2.94967
$\pi/3$	5.00890	4.43448	3.69494	3.43613
$\pi/2$	5.58757	4.95119	4.12745	3.83859
π	0.04412	0.03921	0.03269	0.03041
X		$-\left(\frac{\partial \theta}{\partial Y}\right)_{Y=0}$		
	$H = 0.1$	$H = 1.0$	$H = 4.0$	$H = 6.0$
$\pi/6$	0.91920	0.83795	0.72528	0.68347
$\pi/4$	0.99900	0.91177	0.78974	0.74430
$\pi/3$	1.04965	0.95875	0.83082	0.78310
$\pi/2$	1.08792	0.99431	0.86196	0.81250
π	0.21269	0.19725	0.17585	0.16825

Zia Ullah: Performed the experiments; Analyzed and interpreted the data; Contributed reagents, materials, analysis tools or data; Wrote the paper.

Abid Hussanan; Taher Labidi: Analyzed and interpreted the data; Contributed reagents, materials, analysis tools or data; Wrote the paper.

Lioua Kolsi: Conceived and designed the experiments; Analyzed and interpreted the data; Contributed reagents, materials, analysis tools or data; Wrote the paper.

Data availability statement

No data was used for the research described in the article.

Declaration of competing interest

The authors declare that they have no known competing financial interests or personal relationships that could have appeared to influence the work reported in this paper.

Acknowledgement

Princess Nourah bint Abdulrahman University Researchers Supporting Project number (PNURSP2023R41), Princess Nourah bint Abdulrahman University, Riyadh, Saudi Arabia.

References

[1] P. Forchheimer, Wasserbewegung durch boden, Z. Ver. Dtsch. Ing. 45 (1901) 1782–1788.
[2] M. Muskat, The flow of homogeneous fluids through porous media, Soil Sci. 46 (2) (1938) 169.
[3] H. Upreti, A.K. Pandey, M. Kumar, O.D. Makinde, Ohmic heating and non-uniform heat source/sink roles on 3D Darcy–Forchheimer flow of CNTs nanofluids over a stretching surface, Arab. J. Sci. Eng. 45 (9) (2020) 7705–7717.
[4] M. Ramzan, H. Gul, M. Zahri, Darcy-Forchheimer 3D Williamson nanofluid flow with generalized Fourier and Fick's laws in a stratified medium, Bull. Pol. Acad. Sci. Tech. Sci. 68 (2) (2020).
[5] T. Hayat, F. Haider, T. Muhammad, A. Alsaedi, An optimal study for Darcy-Forchheimer flow with generalized Fourier's and Fick's laws, Results Phys. 7 (2017) 2878–2885.
[6] H. Upreti, N. Joshi, A.K. Pandey, S.K. Rawat, Numerical solution for Sisko nanofluid flow through stretching surface in a Darcy–Forchheimer porous medium with thermal radiation, Heat Transfer 50 (7) (2021) 6572–6588.
[7] M.A. Sadiq, M. Waqas, T. Hayat, Importance of Darcy-Forchheimer relation in chemically reactive radiating flow towards convectively heated surface, J. Mol. Liq. 248 (2017) 1071–1077.
[8] M. Khan, T. Salahuddin, M.Y. Malik, Implementation of Darcy–Forchheimer effect on magnetohydrodynamic Carreau–Yasuda nanofluid flow: application of Von Kármán, Can. J. Phys. 97 (6) (2019) 670–677.
[9] B. Nagaraja, B.J. Gireesha, D.O. Soumya, F. Almeida, Characterization of MHD convective flow of Jeffrey nanofluid driven by a curved stretching surface by employing Darcy–Forchheimer law of porosity, Waves Random Complex Media (2022) 1–20.
[10] M.A.Z. Raja, Z. Khan, S. Zuhra, N.I. Chaudhary, W.U. Khan, Y. He, M. Shoaib, Cattaneo-christov heat flux model of 3D hall current involving bioconvection nanofluidic flow with Darcy-Forchheimer law effect: backpropagation neural networks approach, Case Stud. Therm. Eng. 26 (2021), 101168.
[11] A.V. Shenoy, Darcy-Forchheimer natural, forced, and mixed convection heat transfer in non-Newtonian power-law fluid-saturated porous media, Transport Porous Media 11 (3) (1993) 219–241.
[12] H. Pan, H. Rui, Mixed element method for two-dimensional Darcy-Forchheimer model, J. Sci. Comput. 52 (3) (2012) 563–587.
[13] N. Riley, The heat transfer from a sphere in free convective flow, Comput. Fluids 14 (3) (1986) 225–237.
[14] M. Ashraf, A. Fatima, R.S.R. Gorla, Periodic momentum and thermal boundary layer mixed convection flow around the surface of a sphere in the presence of viscous dissipation, Can. J. Phys. 95 (10) (2017) 976–986.
[15] M. Ashraf, A. Fatima, Numerical simulation of the effect of transient shear stress and the rate of heat transfer around different positions of sphere in the presence of viscous dissipation, J. Heat Tran. 140 (6) (2018) 701–7012.
[16] M. Ashraf, A. Khan, R.S.R. Gorla, Natural convection boundary layer flow of nanofluids around different stations of the sphere and into the plume above the sphere, Heat Tran. Asian Res. 48 (3) (2019) 1127–1148.
[17] A. Abbas, M. Ashraf, Y. Chu, S. Zia, I. Khan, K.S. Nisar, Computational study of the coupled mechanism of thermophoretic transportation and mixed convection flow around the surface of a sphere, Molecules 25 (11) (2020) 2694.
[18] A. Abbas, A. Muhammad, Combined effects of variable viscosity and thermophoretic transportation on mixed convection flow around the surface of a sphere, Therm. Sci. 24 (6B) (2020) 4089–4101.
[19] M. Ashraf, A. Abbas, A. Ali, Z. Shah, H. Alrabaiah, E. Bonyah, Numerical simulation of the combined effects of thermophoretic motion and variable thermal conductivity on free convection heat transfer, AIP Adv. 10 (8) (2020), 085005.
[20] A. Abbas, M. Ashraf, A.J. Chamkha, Combined effects of thermal radiation and thermophoretic motion on mixed convection boundary layer flow, Alex. Eng. J. 60 (3) (2021) 3243–3252.
[21] M. Ashraf, A. Abbas, S. Zia, Y.M. Chu, I. Khan, K.S. Nisar, Computational analysis of the effect of nano particle material motion on mixed convection flow in the presence of heat generation and absorption, CMC Comput. Mater. Continua 65 (2) (2020) 1809–1823.
[22] M. Ashraf, A. Abbas, H.F. Oztop, K.S. Nisar, I. Khan, Computations of mixed convection slip flow around the surface of a sphere: effects of thermophoretic transportation and viscous dissipation, Heat Transfer 50 (7) (2021) 7349–7362.
[23] R. Cortell, A numerical tackling on Sakiadis flow with thermal radiation, Chin. Phys. Lett. 25 (4) (2008) 1340.
[24] L. Ali, B. Ali, M.B. Ghori, Melting effect on Cattaneo–Christov and thermal radiation features for aligned MHD nanofluid flow comprising microorganisms to leading edge: FEM approach, Comput. Math. Appl. 109 (2022) 260–269.
[25] L. Ali, B. Ali, X. Liu, S. Ahmed, M.A. Shah, Analysis of bio-convective MHD Blasius and Sakiadis flow with Cattaneo-Christov heat flux model and chemical reaction, Chin. J. Phys. 77 (2022) 1963–1975.
[26] L. Ali, B. Ali, X. Liu, T. Iqbal, R.M. Zulqarnain, M. Javid, A comparative study of unsteady MHD Falkner–Skan wedge flow for non-Newtonian nanofluids considering thermal radiation and activation energy, Chin. J. Phys. 77 (2022) 1625–1638.
[27] L. Ali, Y. Wang, B. Ali, X. Liu, A. Din, Q. Al Mdallal, The function of nanoparticle's diameter and Darcy-Forchheimer flow over a cylinder with effect of magnetic field and thermal radiation, Case Stud. Therm. Eng. 28 (2021), 101392.
[28] M. Tamoor, M. Waqas, M.I. Khan, A. Alsaedi, T. Hayat, Magnetohydrodynamic flow of Casson fluid over a stretching cylinder, Results Phys. 7 (2017) 498–502.
[29] P.K. Pattnaik, S.R. Mishra, A.K. Barik, A.K. Mishra, Influence of chemical reaction on magnetohydrodynamic flow over an exponential stretching sheet: a numerical study, Int. J. Fluid Mech. Res. 47 (3) (2020) 217–228.
[30] F. Mabood, W.A. Khan, A.M. Ismail, MHD flow over exponential radiating stretching sheet using homotopy analysis method, J. King Saud Univ.-Eng. Sci. 29 (1) (2017) 68–74.
[31] T. Salahuddin, M.Y. Malik, A. Hussain, S. Bilal, M. Awais, MHD flow of Cattanneo–Christov heat flux model for Williamson fluid over a stretching sheet with variable thickness: using numerical approach, J. Magn. Magn Mater. 401 (2016) 991–997.
[32] K.A. Kumar, J.R. Reddy, V. Sugunamma, N. Sandeep, Magnetohydrodynamic Cattaneo-Christov flow past a cone and a wedge with variable heat source/sink, Alex. Eng. J. 57 (1) (2018) 435–443.
[33] A.S. Dogonchi, D.D. Ganji, Impact of Cattaneo–Christov heat flux on MHD nanofluid flow and heat transfer between parallel plates considering thermal radiation effect, J. Taiwan Inst. Chem. Eng. 80 (2017) 52–63.
[34] M.Y. Malik, M. Khan, T. Salahuddin, I. Khan, Variable viscosity and MHD flow in Casson fluid with Cattaneo–Christov heat flux model: using Keller box method, Eng. Sci. Technol. Int. J. 19 (4) (2016) 1985–1992.
[35] A. Kay, H.K. Kuiken, J.H. Merkin, Boundary-layer analysis of the thermal bar, J. Fluid Mech. 303 (1995) 253–278.
[36] E.M. Sparrow, J.L. Gregg, Details of Exact Low Prandtl Number Boundary-Layer Solutions for Forced and for Free Convection, 1959. NASA-MEMO-2-27-59E.
[37] A. Rahimi, A. DehghanSaee, A. Kasaeipoor, E. HasaniMalekshah, A comprehensive review on natural convection flow and heat transfer: the most practical geometries for engineering applications, Int. J. Numer. Methods Heat Fluid Flow 29 (3) (2019) 834–877.
[38] A.S. Dogonchi, T. Tayebi, N. Karimi, A.J. Chamkha, H. Alhumade, Thermal-natural convection and entropy production behavior of hybrid nanoliquid flow under the effects of magnetic field through a porous wavy cavity embodies three circular cylinders, J. Taiwan Inst. Chem. Eng. 124 (2021) 162–173.
[39] N. Biswas, N.K. Manna, A.J. Chamkha, Effects of half-sinusoidal nonuniform heating during MHD thermal convection in Cu–Al 2 O 3/water hybrid nanofluid saturated with porous media, J. Therm. Anal. Calorim. 143 (2021) 1665–1688.
[40] M.M. Bhatti, O.A. Bég, R. Ellahi, T. Abbas, Natural convection non-Newtonian EMHD dissipative flow through a microchannel containing a non-Darcy porous medium: homotopy perturbation method study, Qual. Theory Dyn. Syst. 21 (4) (2022) 97.
[41] M.M. Alam, M.A. Alim, M.M. Chowdhury, Viscous dissipation effects on MHD natural convection flow over a sphere in the presence of heat generation, Nonlinear Anal. Model Control 12 (4) (2007) 447–459.
[42] M. Miraj, M.A. Alim, M.A.H. Mamun, Effect of radiation on natural convection flow on a sphere in presence of heat generation, Int. Commun. Heat Mass Tran. 37 (6) (2010) 660–665.